



# Fluid evolution in zoned Cordilleran polymetallic veins

## Insights from microthermometry and LA-ICP-MS of fluid inclusions

**Journal Article****Author(s):**

Catchpole, Honza; Kouzmanov, Kalin; Fontboté, Lluís; [Guillong, Marcel](#) ; [Heinrich, Christoph A.](#) 

**Publication date:**

2011-02

**Permanent link:**

<https://doi.org/10.3929/ethz-b-000032542>

**Rights / license:**

[Creative Commons Attribution-NonCommercial-NoDerivatives 4.0 International](#)

**Originally published in:**

Chemical Geology 281(3-4), <https://doi.org/10.1016/j.chemgeo.2010.12.016>

This is the Green Open Access version of: Catchpole H., Kouzmanov, K., Fontboté L., Guillong M. and Heinrich, C. A. (2011). Fluid evolution in zoned Cordilleran polymetallic veins – insights from microthermometry and LA-ICP-MS of fluid inclusions. *Chemical geology*, vol. 281, p. 293-304. Original publication see: <https://doi.org/10.1016/j.chemgeo.2010.12.016>

## **Fluid evolution in zoned Cordilleran polymetallic veins – insights from microthermometry and LA-ICP-MS of fluid inclusions**

**Honza Catchpole<sup>a</sup>, Kalin Kouzmanov<sup>a</sup>, Lluís Fontboté<sup>a</sup>, Marcel Guillong<sup>b</sup> and Christoph A. Heinrich<sup>b</sup>**

<sup>a</sup>Earth and Environmental Sciences Section, University of Geneva, 1205 Geneva, Rue des Maraîchers 13, Switzerland (Kalin.Kouzmanov@unige.ch; Lluís.Fontbote@unige.ch)

<sup>b</sup>Institute of Geochemistry and Petrology, Department of Earth Sciences, ETH Zurich, 8092 Zurich, Switzerland (guillong@erdw.ethz.ch; heinrich@erdw.ethz.ch)

*Corresponding author:*

email: Honza.Catchpole@unige.ch

phone: +41765011039

fax: +41223793210

### **Abstract**

Fluid inclusion analysis through the paragenetic sequence of one symmetrically zoned vein sample is used to reconstruct the P-T-X fluid evolution of a porphyry intrusion-related Cordilleran polymetallic vein from Morococha, central Peru. Results record an evolution from initial deep-seated precipitation of quartz-pyrite and base metal sulphides to final near-surface deposition of carbonates, demonstrating progressive mineralisation during uplift and erosion. This is the first detailed study addressing meso- to epithermal Zn-Pb-Ag-Cu-rich ore in a magmatic-hydrothermal system by combination of fluid inclusion microthermometry with laser ablation inductively coupled plasma mass-spectrometry (LA-ICP-MS) quantifying metal, as well as sulphur concentrations in the evolving hydrothermal fluid.

Scanning electron microscopy cathodoluminescence (SEM-CL) imaging of quartz and detailed transmitted- and reflected-light petrography provide textural evidence that early, moderately saline (4-5 wt% NaCl eq.) and CO<sub>2</sub>-bearing fluids with homogenisation temperatures of 340° - 380°C precipitate Cu-bearing minerals. In this open hydrothermal system the fluids record increasingly lower salinities, CO<sub>2</sub> contents and temperatures, while Zn-, Pb-, and Ag sulphides precipitate. Fluids related to early precipitation in the vein have metal contents of several 1000 µg/g S and Fe, over 1000 µg/g Cu, 100 µg/g Pb, 10 µg/g Ag, and several 100 µg/g Zn. Sulphur concentrations in the fluid are sufficiently high to precipitate all metals in solution as sulphides. The latest generation of fluid inclusions associated with abundant carbonate precipitation in the centre of the vein have homogenisation temperatures ranging from 260° to 220°C, low metal concentrations, and no measurable CO<sub>2</sub>.

During vein formation, cooling and several kilometres of erosion resulted in “telescoping” of consecutively precipitated mineral assemblages. The deep input fluid dominating in the early vein stage is interpreted to be of magmatic origin, most likely a single phase magmatic fluid of intermediate salinity and density. It cooled to an aqueous liquid, separated minor CO<sub>2</sub>-rich vapour, and was eventually diluted by meteoric water in the late stages of vein formation when the progressively eroded land surface was only several hundred meters above the vein location.

### **Keywords**

Fluid inclusions; Cordilleran; polymetallic vein; fluid evolution; metal zonation; LA-ICP-MS

## **1. Introduction**

Porphyry-related base metal mineralisation is an important Zn-Pb-Ag-Cu ore type, usually occurring as meso-epithermal veins and massive manto- and chimney-type carbonate replacement bodies. These ores are variably described as Cordilleran, Butte-type, or high and/or intermediate sulphidation epithermal deposits, and are characteristic of the late stages of porphyry copper systems (Meyer et al., 1968; Guilbert and Park, 1986; Bartos, 1989; Einaudi et al., 2003; Sillitoe, 2010). Mineral zonation is a common feature observed during field mapping and mine exploration assaying, and occurs from the small scale of individual base metal veins through large replacement ore bodies to entire ore deposits or mine districts. Classic examples include Casapalca (Rye and Sawkins, 1974), Butte (Meyer et al., 1968), Colquijirca (Bendezú and Fontboté, 2009), Morococha (McLaughlin and Graton, 1935; Cerro de Pasco Copper Corporation, 1948; Petersen, 1965; Catchpole et al., 2008). These deposits and districts typically show a Cu-rich core area, Zn-Pb-Mn-Ag dominated ores in an intermediate to external position and in places As-Sb-Ag-Hg-Au ores towards the outermost areas. The processes controlling metal zonation have been studied in experiments (Hemley et al., 1992; Hemley and Hunt, 1992; Seward and Barnes, 1997). However, the zonation as a function of the chemical evolution of the hydrothermal fluid by in situ fluid inclusion analysis has not been clearly demonstrated to date.

The combination of microthermometry and LA-ICP-MS applied to fluid inclusions has proven to be a powerful tool in understanding ore forming processes in porphyry systems. Several studies document fluid evolution leading to mineralised Cu-(Mo-Au) porphyries (Audétat et al., 1998; Ulrich et al., 1999; Rusk et al., 2004; Klemm et al., 2007; Landtwing et al., 2010) and also porphyry-related base and precious metal epithermal deposits (Heinrich et al., 2004; Wallier et al., 2006; Pudack et al., 2009; Kouzmanov et al., 2010).

In this study we have taken one internally well zoned sample of a Zn-Pb-Ag-Cu-bearing vein from the central part of the polymetallic Morococha district, central Peru, and performed detailed microthermometry and LA-ICP-MS studies of fluid inclusion assemblages throughout the vein paragenesis. Temperature, salinity, metal, sulphur, and other element concentrations in the hydrothermal fluid yield snapshots of the physical and chemical evolution of the ore-forming fluid, and provide insights into metal transport and precipitation mechanisms of economically important Zn-Pb-Ag-Cu-bearing ore minerals in a magmatic-hydrothermal system.

## 2. Geology and vein paragenesis

The Morococha district (Fig. 1) is located in the Western Cordillera of the Central Peruvian Andes and is dominated by barren, and mineralised Cu-Mo and Cu-(Au) porphyry bodies of Miocene age, ranging from 14.1 to 7.7 My (Beuchat, 2003; Bendezú et al., 2008; Kouzmanov et al., 2008). The dioritic to granodioritic porphyries intrude into Permo-Triassic volcano-sedimentary rocks of mostly andesitic composition (Mitu Group), and Triassic-Jurassic (Pucará Group) and Late-Cretaceous sedimentary carbonate formations. Steeply dipping Cordilleran Zn-Pb-Ag-Cu-bearing veins are hosted by NNE to ENE trending fractures. These veins cross-cut the porphyry intrusions and all other lithologies on a district scale (Fig. 1).

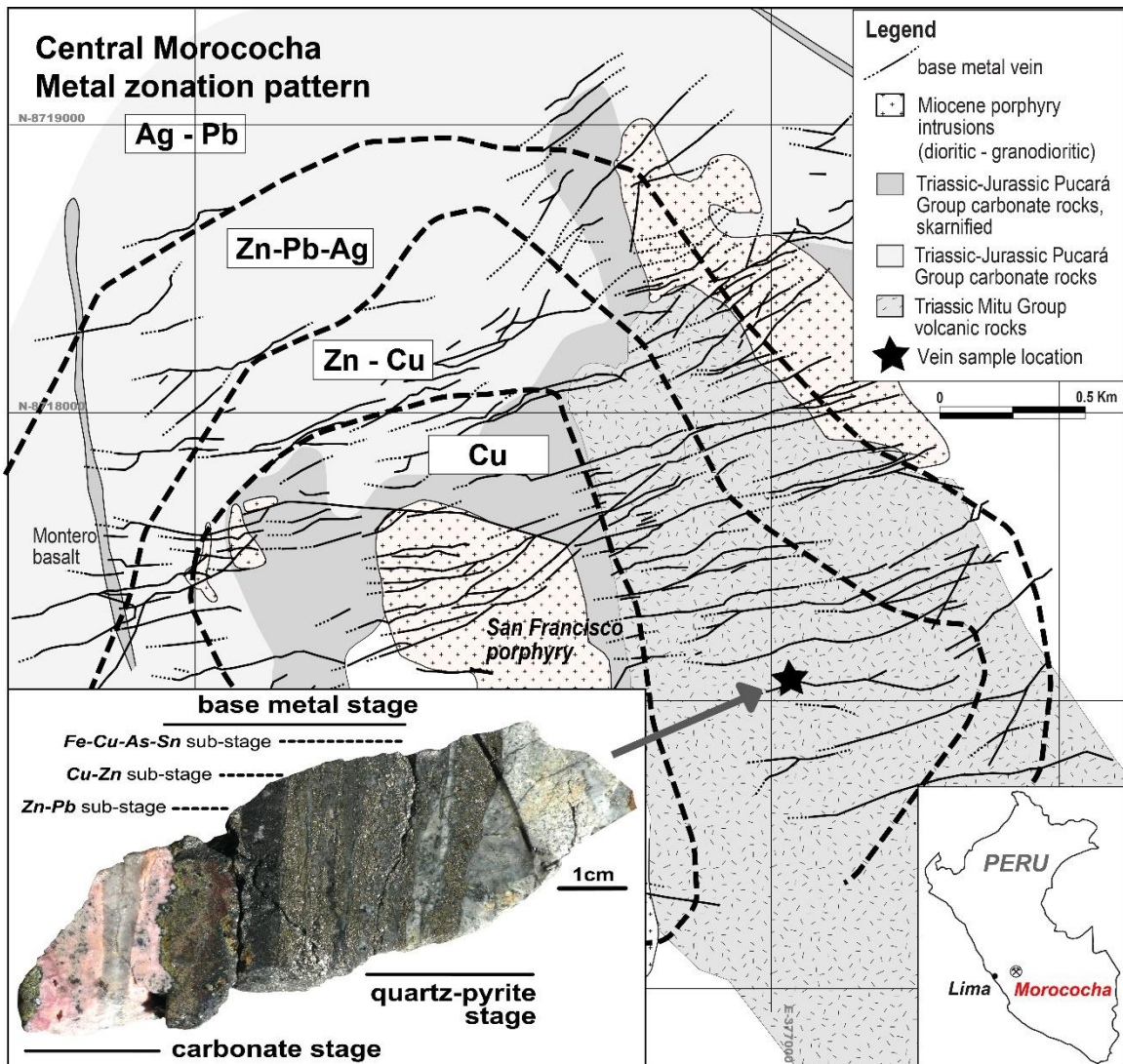


**Fig. 1.** Geological map of mine level 400 (4375 m.a.s.l.) showing Cordilleran polymetallic veins cross-cutting porphyries and volcanic-sedimentary rocks in the central part of the Morococha district (compiled from geological maps of the Cerro de Pasco Copper Corp. (1920 - 1960), Centromin Peru and Pan American Silver Corp). A metal zonation pattern is indicated by dashed lines. The vein sample used for this study is illustrated with paragenetic (sub-)stages and sampling location.

The base metal vein sample used in this study is taken from an underground mine working of Vein Jackeline (200 m below surface) in the base metal-rich central part of the Morococha district (Fig. 1). Three main paragenetic stages can be distinguished: an early barren quartz-pyrite stage, a composite base metal stage, and a late carbonate stage. Early in the base metal stage, pyrite and small amounts of enargite ( $\text{Cu}_3\text{AsS}_4$ ) and stannoidite ( $\text{Cu}_8\text{Fe}_2(\text{Fe,Zn})\text{Sn}_2\text{S}_{12}$ ) precipitate in the Fe-Cu-As-Sn sub-stage. Tennantite and minor sphalerite follow in the Cu-Zn sub-stage. Fe-poor sphalerite and galena precipitate as the Zn-Pb sub-stage of base metal mineralisation. Economically important Ag-bearing minerals are the tennantite-tetrahedrite, and small amounts of hessite ( $\text{Ag}_2\text{Te}$ ) occurring as inclusions in Ag-poor galena. The first two stages are associated with sericitic alteration of the andesite host rock (Mitu Group), whereas the neutral carbonate stage fluids do not affect the host.

The metal zonation recognised in single veins, with Cu- and Fe-bearing minerals precipitating early and Zn, Pb, Ag, and Mn minerals precipitating later in the paragenetic sequence, is also displayed by the district-scale distribution of main metals in base metal lodes in the Morococha district (Fig. 1). A Cu-rich core area overprints the sub-economic San Francisco Cu-Mo porphyry intrusion, while Zn, Pb, Ag and Mn-bearing ores are increasingly important towards external parts of the district (Cerro de Pasco Copper Corporation, 1948; Petersen, 1965). Rhodochrosite of the carbonate stage is absent in the Cu-rich core area. The base metal vein used for this study was sampled from the Zn-Cu zone (Fig. 1).

### 3. Analytical methods

Fluid inclusion assemblages (Goldstein and Reynolds, 1994) were chosen from three doubly polished 150 – 200  $\mu\text{m}$  thick sections prepared from the vein after careful petrographic study. Heating and freezing experiments were conducted with a Linkam heating-freezing stage (THMSG 600) mounted on a DMLB Leica microscope and calibrated using SYN FLINC synthetic fluid inclusions (Sterner and Bodnar, 1984) at  $-56.6^\circ\text{C}$ ,  $0.0^\circ\text{C}$ ,  $274.1^\circ\text{C}$ . A total of 194 fluid inclusions in 27 fluid inclusion assemblages (FIAs) were measured (Table 1). Ice melting,  $\text{CO}_2$  clathrate melting, and homogenisation temperatures ( $T_h$ ) obtained by microthermometry on individual fluid inclusions are repeatable. No visible evidence of post-entrapment modification is found in the samples. Salinities in wt% NaCl equivalent (eq.) and minimum pressures of entrapment were calculated using equations of Zhang and Frantz (1987) and Bodnar and Vityk (1994), the SoWat software (Driesner, 2007), and Flincor software (Brown, 1989). For  $\text{CO}_2$ -bearing fluid inclusions with optically distinguishable clathrate formation (clathrate melting temperature higher than ice melting temperature), salinities (wt%),  $\text{CO}_2$  content (mol%), and pressures (bar) were calculated using the ICE and LONER15 software and equations from Bakker (1997) and Duan et al. (1992). Ice- and clathrate melting temperatures and the liquid-vapour (l/v) ratios of the fluid inclusions are required for these calculations. Estimation of the l/v ratios is the biggest source of error and is therefore calculated with a 10% variation above and below the actual observed ratio.

Fluid inclusion petrography is supported by scanning electron microscopy cathodoluminescence (SEM-CL) images to better understand the paragenetic context of the studied FIAs. The SEM-CL images were acquired at the University of Lausanne using a CamScan MV2300 SEM. For determining the presence of  $\text{CO}_2$ , Raman microspectroscopy measurements (LABRAM with 632.8 nm He-Ne laser, University of Geneva) on single fluid inclusions and crushing tests were performed using a simple hinge crushing device on small

quartz fragments in oil as described by Roedder (1984). Detection limits for these methods are 0.2 mol% CO<sub>2</sub> (Bodnar et al., 1985) and 0.1 mol% CO<sub>2</sub> (Rosso and Bodnar, 1995), respectively.

Chemical composition of single fluid inclusions (Na, K, Cs, S, Fe, Cu, Zn, Pb, Sb, As, and Ag) were measured using an 193 nm Excimer ArF laser (Geolas, ETH prototype) coupled with an Elan 6100 DRC quadrupole ICP-MS for multi element analysis at the ETH Zurich (Günther et al., 1998; Heinrich et al., 2003). Element concentrations for 105 fluid inclusions from 18 FIAs were obtained (Table 2; fluid inclusion size >15 µm, 3-10 fluid inclusions/assemblage). Salinities calculated from microthermometry measurements (for 90% of all ablated fluid inclusions) prior to ablation are used as internal standards for each of the individually ablated fluid inclusion, applying an empirical correction for cations other than sodium, especially potassium (Heinrich et al., 2003). The average salinity of all fluid inclusions of a FIA is taken as an internal standard if no salinity was obtained by microthermometry for an individual fluid inclusion. For the sphalerite and rhodochrosite hosts, S (32.4 wt%) and Mn (47.2 wt%) values, respectively, were obtained by electron microprobe analyses (JEOL 8200 Superprobe, University of Lausanne) and used as internal standard for the host mineral correction. A near pure quartz (99.9 wt% SiO<sub>2</sub>) host is assumed for fluid inclusions in quartz. Sulphur was measured, the data reduced and concentrations calculated according to Guillong et al. (2008a) and Seo et al. (2009) using the SILLS software (Guillong et al., 2008b). Elements are reported as total concentrations and also as element/Na ratios (Table 3) in order to check internal consistency of the total concentrations calculated, especially for FIAs with an unknown amount of CO<sub>2</sub> that biases measured salinity.

**Table 1**

Microthermometric data for 27 fluid inclusion assemblages from the KMO-7-241 Jackeline vein sample

Assemblages	Group	Host	Type	Tm (ice) (°C)	n	Tm (clath) (°C)	n	Salinity (eq. NaCl wt%)	Density (ice) (g/cm <sup>3</sup> )	CO2 (mol %)	Vapour bubble (%)	Th (°C)	n	Minimum pressure (p) (bar)
241a_2-B	L2	qz	PS	-2.3 ± 0.1	8			3.9 ± 0.1	0.87 ± 0.01	<0.13	10	226 ± 4	6	22 ± 2
241a_2-C	L2	qz	PS	-3.3 ± 0.0	4			5.4 ± 0.0	0.88 ± 0.01	<0.13	10	224 ± 5	4	22 ± 2
241a_5-A	L2	carb	P	-2.4 ± 0.4	5			4.0 ± 0.6	0.83 ± 0.02	<0.13	15	253 ± 8	8	39 ± 9
241a_5-B	L2	carb	P	-1.5 ± 0.3	7			2.5 ± 0.5	0.82 ± 0.01	<0.13	15	249 ± 4	16	34 ± 2
241a_6-A	L2	carb	P	-3.4 ± 0.4	6			5.5 ± 0.6	0.85	<0.13	10-15	248 ± 5	9	33 ± 1
241a_11-A	L2	qz	P	-1.1 ± 0.1	6			2.0 ± 0.1	0.85 ± 0.01	<0.13	10-15	227 ± 6	7	23 ± 3
241a_3-A	L2	qz	P	-1.2 ± 0.1	8			2.0 ± 0.2	0.84 ± 0.01	<0.13	10-15	232 ± 4	9	25 ± 2
241a_3-B	L2	qz	P	-1.7	1			2.9		<0.13	10-15	259	1	44
241a_4-A	L2	qz	P	-1.2 ± 0.1	6			2.1 ± 0.2	0.85 ± 0.01	<0.13	10	225 ± 9	6	22 ± 4
241a_4-B	L2	qz	P	-1.3 ± 0.2	5			2.3 ± 0.3	0.86 ± 0.01	<0.13	10	220 ± 4	5	20 ± 2
241a_16	L2	sl	S	-1.4 ± 0.2	4			2.4 ± 0.2	0.82 ± 0.01	<0.13	10-15	246 ± 8	3	33 ± 5
241a_7	L2	sl	S	-1.3 ± 0.3	5			2.3 ± 0.5	0.83	<0.13	10-15	241 ± 1	5	30 ± 1
241a_13-A	L2	qz	S-boiling	-2.7 ± 0.2	6			4.5 ± 0.3	0.83 ± 0.01	<0.13	20-25	254 ± 4	7	39 ± 3
241a_8-C	L2	qz	S-boiling	-2.5 ± 0.1	8			4.2 ± 0.1	0.82 ± 0.01	<0.13	20-25	260 ± 5	12	<b>43 ± 5</b>
241a_8-D	L2	qz	S	-1.8 ± 0.2	5			3.1 ± 0.3	0.81 ± 0.01	<0.13	20-25	260 ± 8	8	40 ± 1
241_1_3-G	L2	qz	S-boiling	-1.4 ± 0.2	5			2.0 ± 1.0	0.78 ± 0.06	<0.13	10-15	266 ± 10	3	53 ± 26
241_1_5-A	L1	qz	S	-5.0 ± 0.8	12	5.8 ± 0.3	7	4.4 ± 0.2	0.71 ± 0.04	4.20 ± 0.5	35-40	343 ± 8	8	505 ± 116
241_1_5-B	L1	qz	S	-2.9 ± 0.4	6			4.8 (2.2) ± 0.6		0.0 (1.6)	20-25	326 ± 17	6	
241_2_5-A	L1	qz	S	-2.1 ± 0.4	13			2.7 (1.0) ± 0.6		0.0 (1.6)	20	316 ± 6	12	
241_2_5-C	L1	qz	S-boiling	-2.0 ± 0.1	5			3.4 ± 0.2	0.68 ± 0.01	0.0 (1.6)	20	327 ± 2	4	<b>117</b>
241_2_7-B	L1	qz	S	-5.7 ± 0.4	6	3.0 ± 0.0	2	4.8 ± 0.1	0.68 ± 0.04	3.30 ± 0.4	35	359 ± 20	5	487 ± 142
241_2_7-C	L1	qz	S	-2.2 ± 0.2	3			3.8 (1.1) ± 0.3	0.72 ± 0.01	0.0 (1.6)	25	319 ± 10	4	
241_2_7-D	L1	qz	S	-4.5 ± 0.5	11	2.6 ± 0.4	6	4.9 ± 0.1	0.68 ± 0.01	3.10 ± 0.5	35	357 ± 9	11	414 ± 69
241a_9-B	L1	qz	S	-4.3 ± 0.6	11	3.0 ± 0.0	3	4.6 ± 0.2	0.55	4.12 ± 0.8	50	373 ± 7	12	340 ± 15
241a_8-B	L1	qz	S	-4.2 ± 0.1	3	3.0 ± 0.0	2	4.4 ± 0.3	0.45	5.06	55-60	382 ± 3	6	295 ± 7
241a_8-G	L1	qz	S	-3.2 ± 0.3	6	1.8 ± 0.0	2	4.7 ± 0.3	0.38	5.17 ± 1.4	60-65	355 ± 18	9	
241a_8-A	V	qz	S	-1.6 ± 0.0	2			2.7 (0.2) ± 0.0			75	384 ± 6	8	
Total: 27					167		22						194	

Salinities in brackets are calculated assuming 1.6 mol % CO<sub>2</sub>. Absolute pressures obtained calculated from boiling FIAs are set bold. Data are reported as assemblage averages with 1σ standard deviation. The number of relevant single measured values (n) are set italic, n.a. = not analysed. Host mineral of fluid inclusion are quartz (qz), sphalerite (sl), or Mn-carbonate (carb). Fluid inclusion trails are primary (P), pseudosecondary (PS), secondary (S), or secondary boiling (S-boiling)



**Table 2**

Element concentrations ( $\mu\text{g/g}$ ) obtained by LA-ICP-MS for 18 fluid inclusion assemblages from the KMO-7-241 Jackeline vein sample

Assemblages	Group	Na	<i>n</i>	S	<i>n</i>	K	<i>n</i>	Fe	<i>n</i>	Cu	<i>n</i>
241a_2-B	L2	15500 $\pm$ 500	2			400	<i>1</i>			20	<i>1</i>
241a_5-A	L2	14000 $\pm$ 800	2			5500 $\pm$ 400	2				
241a_5-B	L2	8800 $\pm$ 600	7			3700 $\pm$ 800	6			50	<i>1</i>
241a_11-A	L2	7500	<i>1</i>				<i>1</i>				
241a_3-A	L2	7600 $\pm$ 900	<i>11</i>	1200	<i>1</i>	500 $\pm$ 200	8			50 $\pm$ 60	2
241a_3-B	L2	11200	<i>1</i>	2300	<i>1</i>	600	<i>1</i>				
241a_16	L2	4700 $\pm$ 200	7			2000 $\pm$ 500	7	200 $\pm$ 180	2	200 $\pm$ 160	4
241a_7	L2	7700 $\pm$ 1200	8			3200 $\pm$ 800	8		<i>1</i>	190	<i>1</i>
241_1_5-A	L1	16200 $\pm$ 800	9	2000 $\pm$ 400	4	3700 $\pm$ 1700	9	600 $\pm$ 300	2	200 $\pm$ 60	8
241_1_5-B	L1	8000 $\pm$ 2000	8	900 $\pm$ 400	2	2200 $\pm$ 700	8	300	<i>1</i>	180 $\pm$ 200	6
241_2_5-A	L1	3800 $\pm$ 1800	7			1700 $\pm$ 600	7	80	<i>1</i>	100 $\pm$ 30	6
241_2_5-C	L1	11100 $\pm$ 700	5			6000 $\pm$ 2000	5	200	<i>1</i>	270 $\pm$ 200	5
241_2_7-B	L1	16000 $\pm$ 2000	4	5400	<i>1</i>	7000 $\pm$ 6000	4	1500 $\pm$ 1000	2	200 $\pm$ 60	3
241_2_7-D	L1	17700 $\pm$ 1200	8	1500 $\pm$ 700	6	4000 $\pm$ 2000	8	1000 $\pm$ 600	5	400 $\pm$ 200	6
241a_8-A	V	500 $\pm$ 110	7	800 $\pm$ 500	7	500 $\pm$ 300	7	200 $\pm$ 70	5	900 $\pm$ 200	7
241a_8-B	L1	15100 $\pm$ 1700	3	11000 $\pm$ 6000	2	6000 $\pm$ 4000	3	3000 $\pm$ 2500	3	1100	<i>1</i>
241a_8-C	L2	14600 $\pm$ 700	5			5000 $\pm$ 2000	5			240 $\pm$ 100	3
241a_9-B	L1	15100 $\pm$ 900	8	3800 $\pm$ 1900	7	9000 $\pm$ 2000	8	2000 $\pm$ 1400	7	2700 $\pm$ 1800	7

Assemblages	Group	Zn	<i>n</i>	As	<i>n</i>	Ag	<i>n</i>	Sb	<i>n</i>	Cs	<i>n</i>	Pb	<i>n</i>
241a_2-B	L2			90	<i>1</i>			18 $\pm$ 18	2	4 $\pm$ 1	2		
241a_5-A	L2			50	<i>1</i>					20 $\pm$ 2	2		
241a_5-B	L2			70 $\pm$ 50	4	19 $\pm$ 15	2	40 $\pm$ 20	2	16 $\pm$ 2	5	14 $\pm$ 18	2
241a_11-A	L2	40	<i>1</i>	200	<i>1</i>	2	<i>1</i>	70	<i>1</i>	2 $\pm$ 3	2		
241a_3-A	L2	50	<i>1</i>	160 $\pm$ 80	10	30	<i>1</i>	100 $\pm$ 70	9	5 $\pm$ 3	8	6 $\pm$ 3	3
241a_3-B	L2			160	<i>1</i>			180	<i>1</i>	7			
241a_16	L2			70 $\pm$ 40	4	n.a.		15 $\pm$ 16	4	6 $\pm$ 3	7	30 $\pm$ 20	5
241a_7	L2			120 $\pm$ 70	7	n.a.		150 $\pm$ 90	6	11 $\pm$ 4	8		
241_1_5-A	L1	70 $\pm$ 40	6	27 $\pm$ 7	6	1	<i>1</i>	19 $\pm$ 17	8	22 $\pm$ 9	9	30 $\pm$ 20	9
241_1_5-B	L1	210 $\pm$ 150	5	50 $\pm$ 50	5	4 $\pm$ 2	3	10 $\pm$ 5	4	12 $\pm$ 11	8	40 $\pm$ 30	7
241_2_5-A	L1	39 $\pm$ 16	4	22 $\pm$ 13	7	<1	<i>1</i>	5 $\pm$ 2	3	17 $\pm$ 10	7	3 $\pm$ 4	3
241_2_5-C	L1	160	<i>1</i>	30	<i>1</i>	26	<i>1</i>	6	<i>1</i>	12 $\pm$ 11	5	110	<i>1</i>
241_2_7-B	L1	320 $\pm$ 200	2	100 $\pm$ 40	3	10 $\pm$ 2	3	30 $\pm$ 20	3	21 $\pm$ 9	4	150 $\pm$ 90	4
241_2_7-D	L1	150 $\pm$ 60	8	50 $\pm$ 40	7	3 $\pm$ 4	6	50 $\pm$ 70	7	15 $\pm$ 9	8	60 $\pm$ 40	8
241a_8-A	V	20 $\pm$ 7	5	4 $\pm$ 2	4	<1	5	2	3	1	6	5 $\pm$ 3	7
241a_8-B	L1	200	<i>1</i>	180	<i>1</i>	7	<i>1</i>	30 $\pm$ 6	3	27 $\pm$ 4	2	80 $\pm$ 60	3
241a_8-C	L2					26 $\pm$ 17	2	56 $\pm$ 18	2	45 $\pm$ 22	4	27 $\pm$ 17	2
241a_9-B	L1	300 $\pm$ 150	8	50 $\pm$ 30	9	10 $\pm$ 12	8	30 $\pm$ 20	4	13 $\pm$ 4	10	140 $\pm$ 60	8

The number of relevant single measured concentrations (*n*) are set italic, 1 $\sigma$  standard deviation for FIAs, n.a. = not analysed



## 4. Results

### 4.1. *Fluid inclusions petrography*

Fluid inclusions are mostly aqueous liquid-rich (L), hosted in quartz or subordinately in rhodochrosite and sphalerite (Fig. 2). Vapour-rich fluid inclusions are found together with aqueous fluid inclusions in boiling FIAs (Fig. 2c). No salt-saturated fluid inclusions are observed in the vein. Three groups of mostly liquid-rich fluid inclusions are distinguished according to their paragenetic position in the vein, and their l/v ratios. Early fluid inclusions (L<sub>1</sub>) predate the Zn-Pb sub-stage and are mostly secondary, cross-cutting quartz and pyrite of the first mineralisation stage. The l/v ratios of these fluid inclusions is variable, the vapour bubble occupies between 20% and 60% of the total inclusions volume. One FIA (V) has a l/v ratio of 75%, characteristic for high-density vapour-type fluid inclusions. Fluid inclusions (L<sub>2</sub>) postdating the Zn-Pb sub-stage and precipitating together with and after rhodochrosite, are mainly primary with smaller vapour bubbles (10 – 25%) averaging at 15%. Boiling FIAs with vapour and aqueous fluid inclusions are frequently registered in the L<sub>2</sub> group. L<sub>1</sub> fluid inclusions frequently have chalcopyrite daughters / trapped solids (Fig. 2b), and all V fluid inclusions have chalcopyrite daughters. Both L<sub>1</sub> and L<sub>2</sub> can have varying amounts of accidentally trapped fine fibrous muscovite-illite crystals as revealed by Raman microspectroscopy.

Early L<sub>1</sub> and V fluid inclusion trails post-date the quartz-pyrite stage and are coeval with Cu-ore precipitation as shown by following textural evidence: cracks cross-cutting pyrite are filled by tennantite and continue as healed fractures with fluid inclusions trails into quartz, as evidenced by SEM-CL (Fig. 2a). SEM-CL imaging additionally reveals that well zoned quartz from the pyrite-quartz stage has dissolution textures in the rim areas and subsequent quartz re-precipitation prior to first Cu-mineral precipitation (Fig. 2a).

### 4.2. *CO<sub>2</sub> content and microthermometry*

Several L<sub>1</sub> FIAs show CO<sub>2</sub> clathrate formation during freezing experiments, but no liquid CO<sub>2</sub> is observed at ambient temperatures. Using the Raman method, small amounts of CO<sub>2</sub> have been detected in L<sub>1</sub> and V fluid inclusions not showing clathrate formation and occurring prior to rhodochrosite precipitation. However, clathrate formation in the V fluids inclusions can easily be overlooked due to the big vapour bubbles and the amount of CO<sub>2</sub> is not readily determinable. No CO<sub>2</sub> was registered for L<sub>2</sub> fluid inclusions, neither by crushing stage test nor by Raman microspectroscopy.

The presence of CO<sub>2</sub> can have a strong effect on measured ice melting temperatures and significantly depress the melting point of ice. This can result in an important overestimation of the fluid salinity, particularly in the low-salinity range if CO<sub>2</sub> is not noticed and/or not taken in account (Hedenquist and Henley, 1985). Salinities can not be calculated for CO<sub>2</sub>-bearing fluid inclusions without distinguishable clathrate formation. A CO<sub>2</sub> content of 1.5 mol% is considered the minimum amount for clathrate formation following H<sub>2</sub>O-CO<sub>2</sub> phase relationships outlined by Diamond (2001). Therefore, a compositional range of salinities is proposed for CO<sub>2</sub>-bearing fluid inclusions without observable clathrate. The compositional ranges are calculated for a fluid assuming 1.6 mol% CO<sub>2</sub> and a CO<sub>2</sub>-free system as indicated by the dashed gray shaded area in figures 3a and 3b.

**Table 3**

Element ratios (X/Na) obtained by LA-ICP-MS for 18 fluid inclusion assemblages from the KMO-7-241 Jackeline vein sample

Assemblages	Group	S/Na	<i>n</i>	K/Na	<i>n</i>	Fe/Na	<i>n</i>	Cu/Na	<i>n</i>	Zn/Na	<i>n</i>	As/Na	<i>n</i>	Ag/Na	<i>n</i>	Sb/Na	<i>n</i>	Cs/Na	<i>n</i>	Pb/Na	<i>n</i>
241a_2-B	L2			0.02				0.00				0.010				0.0010 ± 0.0012		0.0003 ± 0.0001			
241a_5-A	L2			0.39 ± 0.05								0.004						0.0014			
241a_5-B	L2			0.40 ± 0.11				0.01				0.010 ± 0.010		0.0020 ± 0.0020		0.0040 ± 0.0030		0.0018 ± 0.0003		0.0020 ± 0.0020	
241a_11-A	L2									0.010		0.030		0.0002		0.0090		0.0003 ± 0.0004			
241a_3-A	L2	0.15	<i>1</i>	0.06 ± 0.03	<i>4</i>			0.01 ± 0.010	<i>1</i>	0.010	<i>1</i>	0.020 ± 0.010	<i>5</i>	0.0044		0.0130 ± 0.0090	<i>4</i>	0.0007 ± 0.0006	<i>3</i>	0.0008 ± 0.0003	<i>2</i>
241a_3-B	L2	0.21		0.06								0.014				0.0160		0.0006			
241a_16	L2		<i>7</i>	0.40 ± 0.14	<i>7</i>	0.04 ± 0.04	<i>2</i>	0.04 ± 0.030	<i>4</i>			0.015 ± 0.010	<i>5</i>			0.0030 ± 0.0040	<i>5</i>	0.0013 ± 0.0006	<i>7</i>	0.0060 ± 0.0050	<i>5</i>
241a_7	L2		<i>7</i>	0.41 ± 0.09	<i>8</i>			0.02				0.020 ± 0.010	<i>7</i>			0.0190 ± 0.0120	<i>6</i>	0.0014 ± 0.0005	<i>8</i>		
241_1_5-A	L1	0.12 ± 0.03	<i>3</i>	0.20 ± 0.12	<i>7</i>	0.04 ± 0.02	<i>2</i>	0.01 ± 0.004	<i>7</i>	0.005 ± 0.003	<i>5</i>	0.002 ± 0.000	<i>4</i>	0.0001		0.0010 ± 0.0010	<i>7</i>	0.0014 ± 0.0006	<i>7</i>	0.0020 ± 0.0014	<i>6</i>
241_1_5-B	L1	0.11 ± 0.07	<i>2</i>	0.28 ± 0.06	<i>8</i>	0.06		0.02 ± 0.020	<i>6</i>	0.020 ± 0.020	<i>5</i>	0.010 ± 0.010	<i>5</i>	0.0005 ± 0.0002	<i>3</i>	0.0010 ± 0.0010	<i>4</i>	0.0016 ± 0.0013	<i>8</i>	0.0040 ± 0.0040	<i>7</i>
241_2_5-A	L1			0.45 ± 0.07	<i>7</i>	0.04		0.03 ± 0.010	<i>6</i>	0.010 ± 0.010	<i>4</i>	0.006 ± 0.002	<i>7</i>	0.0001		0.0020 ± 0.0011	<i>3</i>	0.0050 ± 0.0030	<i>7</i>	0.0010 ± 0.0014	<i>3</i>
241_2_5-C	L1			0.50 ± 0.20	<i>4</i>	0.02		0.02 ± 0.020	<i>3</i>	0.010		0.002		0.0023		0.0005		0.0010 ± 0.0010	<i>5</i>	0.0100	
241_2_7-B	L1	0.34		0.50 ± 0.50	<i>4</i>	0.11 ± 0.09	<i>2</i>	0.02 ± 0.002	<i>3</i>	0.020 ± 0.020	<i>2</i>	0.007 ± 0.004	<i>3</i>	0.0006 ± 0.0002	<i>3</i>	0.0020 ± 0.0011	<i>3</i>	0.0013 ± 0.0004	<i>4</i>	0.0100 ± 0.0060	<i>4</i>
241_2_7-D	L1	0.08 ± 0.04	<i>6</i>	0.20 ± 0.12	<i>7</i>	0.06 ± 0.04	<i>5</i>	0.02 ± 0.011	<i>6</i>	0.010 ± 0.003	<i>8</i>	0.003 ± 0.002	<i>7</i>	0.0002 ± 0.0002	<i>6</i>	0.0030 ± 0.0040	<i>7</i>	0.0009 ± 0.0005	<i>8</i>	0.0040 ± 0.0020	<i>8</i>
241a_8-A	V	1.60 ± 0.90	<i>8</i>	1.00 ± 0.80	<i>8</i>	0.30 ± 0.18	<i>6</i>	1.78 ± 0.800	<i>7</i>	0.040 ± 0.010	<i>6</i>	0.010 ± 0.010	<i>5</i>	0.0010 ± 0.0003	<i>6</i>	0.0038 ± 0.0002	<i>4</i>	0.0012 ± 0.0003	<i>7</i>	0.0080 ± 0.0040	<i>8</i>
241a_8-B	L1	0.70 ± 0.35	<i>2</i>	0.40 ± 0.40	<i>3</i>	0.20 ± 0.15	<i>3</i>	0.08		0.010		0.011		0.0005		0.0018 ± 0.0007	<i>2</i>	0.0018 ± 0.0001	<i>3</i>	0.0050 ± 0.0040	<i>2</i>
241a_8-C	L2			0.30 ± 0.20	<i>5</i>			0.02 ± 0.010	<i>3</i>					0.0020 ± 0.0011	<i>2</i>	0.0040 ± 0.0014	<i>2</i>	0.0031 ± 0.0014	<i>4</i>	0.0020 ± 0.0014	<i>2</i>
241a_9-B	L1	0.26 ± 0.12	<i>6</i>	0.60 ± 0.20	<i>8</i>	0.13 ± 0.09	<i>5</i>	0.18 ± 0.130	<i>5</i>	0.020 ± 0.010	<i>8</i>	0.003 ± 0.002	<i>8</i>	0.0005 ± 0.0008	<i>6</i>	0.0020 ± 0.0020	<i>3</i>	0.0009 ± 0.0003	<i>8</i>	0.0090 ± 0.0040	<i>8</i>

The number of relevant single measured concentrations (*n*) are set italic, 1σ standard deviation for FIAs

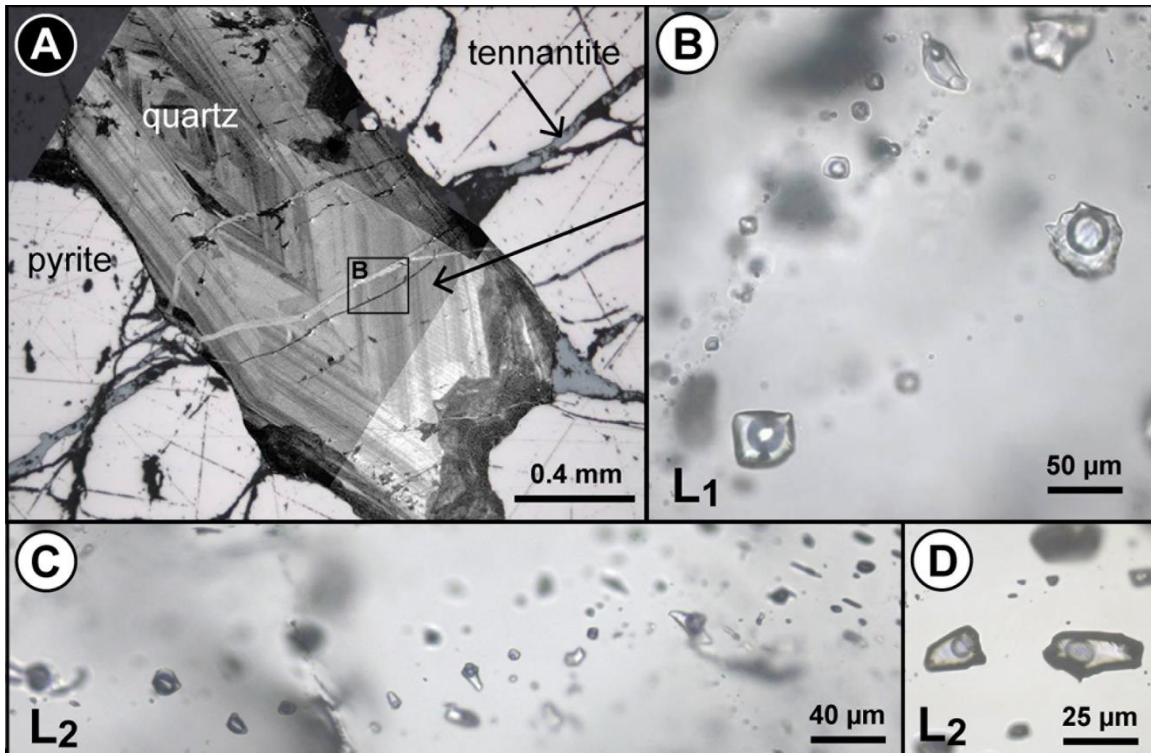


**Fig. 2.** (a) Reflected light microphotograph with tennantite-bearing fractures in pyrite and SEM-CL image of the quartz crystal superimposed, indicating growth zones and healed fractures cross-cutting. (b) Inset from (a) with L<sub>1</sub> fluid inclusions with opaque daughter phases. (c) L<sub>2</sub> quartz hosted boiling FIA. (d) Sphalerite hosted L<sub>2</sub> fluid inclusions.

Microthermometry of early L<sub>1</sub> quartz hosted fluid inclusions, coeval with the precipitation of Cu-minerals, yields moderate salinities and homogenisation temperatures of up to 4.9 wt% NaCl eq. and 382°C, respectively (Fig. 3a). Six L<sub>1</sub> FIAs in the T<sub>h</sub> range 340 - 383°C have similar salinities of 4.4 - 4.9 wt% equivalent NaCl and CO<sub>2</sub> contents of 3.1 to 5.2 mol% (Fig. 3b). With decreasing T<sub>h</sub> both CO<sub>2</sub> content and salinities decrease. In the T<sub>h</sub> range of 300° - 340°C the CO<sub>2</sub> content is below 1.6 mol% indicated by the absence of CO<sub>2</sub> clathrate after ice melting for these moderately dense fluids. L<sub>1</sub> fluid inclusions have elevated to intermediate densities (0.7 - 0.4 g/cm<sup>3</sup>). Two L<sub>1</sub> FIAs show homogenisation to vapour, all others to liquid upon heating. The exact time-relationship among these L<sub>1</sub> FIAs is not known. Therefore they are presented here according to their respective T<sub>h</sub> (Fig. 3a). The V FIA records the highest T<sub>h</sub> (384°C), but lower salinities of 2.7 wt% NaCl eq. with an unknown amount of CO<sub>2</sub>.

All aqueous L<sub>2</sub> fluid inclusions from boiling FIAs hosted in rhodochrosite and quartz are found within the narrow T<sub>h</sub> range 255 - 265°C, and fluid salinity shows a sharp rise of up to 5.5 wt% NaCl eq. for this T<sub>h</sub> range. Because of the low amount of liquid, ice melting and phase homogenisation in vapour L<sub>2</sub> fluid inclusions of boiling FIAs could not be reliably observed during heating-cooling experiments, so these inclusions remain unmeasured in the L<sub>2</sub> boiling FIAs.

Later, post-ore quartz L<sub>2</sub> fluid inclusions have the lowest salinities and T<sub>h</sub> (2.0 - 2.3 wt% NaCl eq. and 220 - 250°C, respectively), which mark the last mineral deposition in the vein. L<sub>2</sub> FIAs in the very last precipitating quartz record a second sharp increase in salinities (up to 5.5 wt% NaCl eq.) and slight increase in T<sub>h</sub> (225°C). Densities for L<sub>2</sub> fluid inclusions are 0.8 - 0.9 g/cm<sup>3</sup>.

Calculated minimum pressures for the CO<sub>2</sub>-bearing L<sub>1</sub> fluid inclusions in the T<sub>h</sub> range 340° - 383°C have a large spread, in some cases ranging from 300 to 600 bars within one FIA. At low CO<sub>2</sub> contents in the H<sub>2</sub>O-CO<sub>2</sub>-NaCl system small changes in total fluid inclusion density and CO<sub>2</sub> can have strong effect on pressure, therefore explaining the large spread in pressures for individual FIAs (Diamond, 2001). The boiling L<sub>2</sub> FIAs have absolute pressures of 39-47 bars.

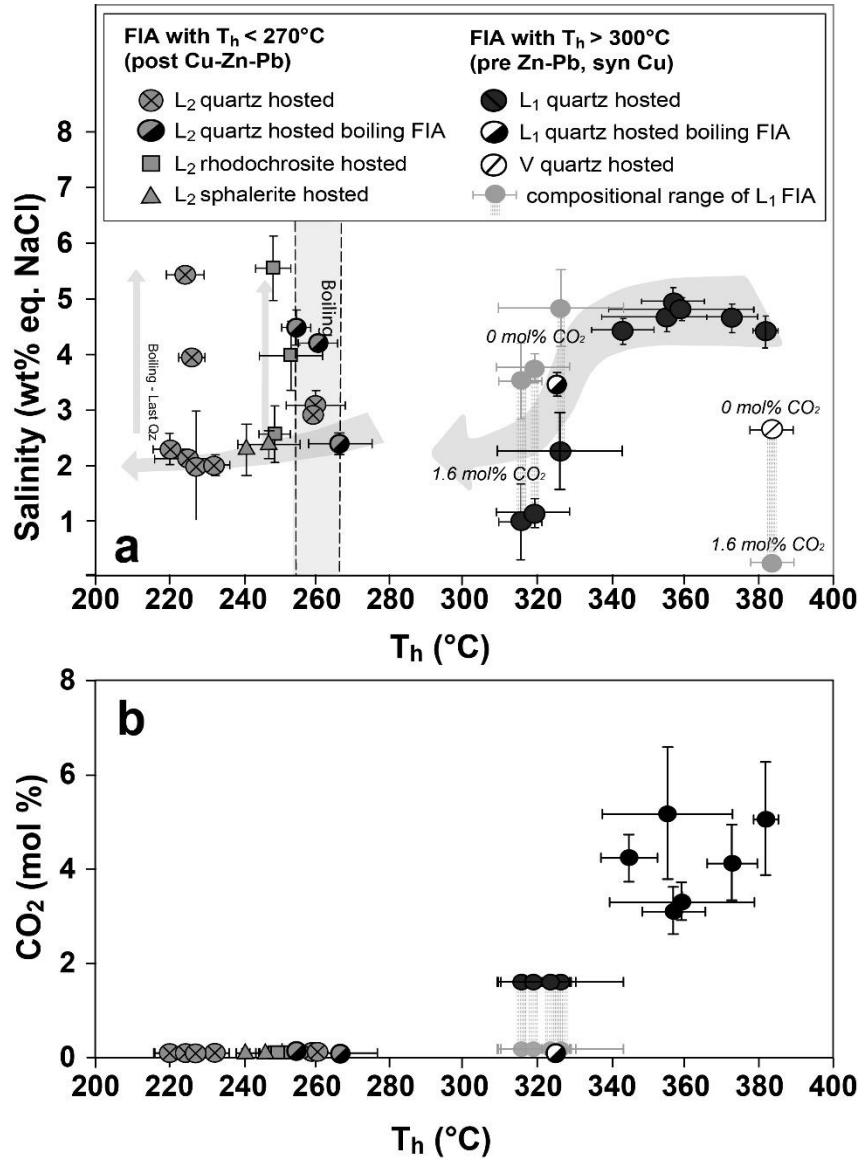


**Fig. 3.** (a) Homogenisation temperatures and salinities for various L<sub>1</sub>, L<sub>2</sub>, and V FIAs hosted in quartz, sphalerite, and rhodochrosite from the studied base metal vein. Values for each FIA are plotted as average with 1 $\sigma$  error bars. FIAs with an uncertain salinity due to the presence of CO<sub>2</sub> have vertical ranges which end upwards into a CO<sub>2</sub>-free salinity and to the bottom into a salinity calculated for a 1.6 mol% CO<sub>2</sub> composition (Hedenquist and Henley, 1985). The shaded T<sub>h</sub> range highlights a boiling temperature zone with several boiling FIAs and small arrows indicate the increased salinities due to boiling. The larger gray arrows indicate the cooling and dilution path of decreasing T<sub>h</sub> and salinity. (b) CO<sub>2</sub> content plotted against T<sub>h</sub> illustrates the decrease of CO<sub>2</sub> from early values of 3.1 - 5.2 mol% to <0.13 mol% for post-boiling temperatures.

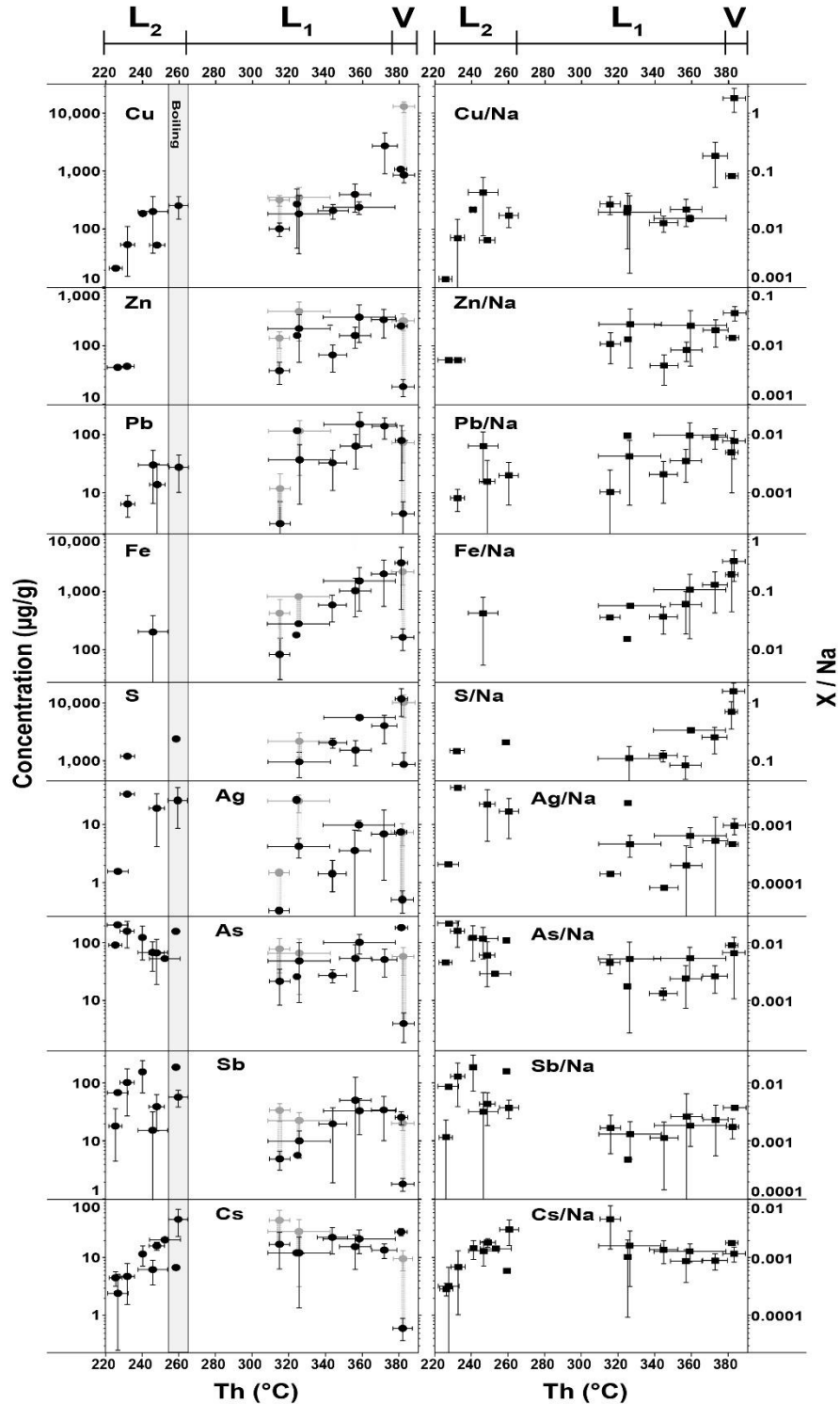


**Fig. 4.** Left column:  $T_h$  versus selected element concentrations for FIAs within the studied vein sample. In general, the evolution of the element concentrations correlates with the decreasing  $T_h$ . Values for each FIA are plotted as mean with  $1\sigma$  error bars. For FIAs where only one measurement is available no vertical error bars are shown. The boiling  $T_h$  range is indicated by a grey vertical zone. Right column:  $T_h$  versus selected element ratios ( $X/Na$ ) for the FIAs, corresponding to the elements in the left column. FIAs are plotted as mean with  $1\sigma$  error bars.

### 4.3. Fluid composition by LA-ICP-MS analyses

Element concentrations plotted against  $T_h$  show similar patterns for their corresponding element/Na ratio (Fig. 4). Concentrations for FIAs with an unknown amount of  $\text{CO}_2$  in the vapour phase are calculated as minimum (1.6 mol%  $\text{CO}_2$ ) and maximum values (no  $\text{CO}_2$ ), connected by vertical grey bars indicating the compositional range for each element (Fig. 4). Even if the precise element concentrations are not known for these FIAs, a comparison of element concentrations and element ratios of other  $L_1$  FIAs shows that element ratios are consistently high, so the real total element concentrations for these FIAs probably plot in the upper part of the vertical grey bars and the  $\text{CO}_2$  content is probably low.

Iron, Cu, Pb, Zn, and S have higher concentrations for the earlier  $L_1$  FIAs compared to  $L_2$  FIAs, both in absolute concentration and relative to Na. Copper and iron show decreasing concentration and ratio trends. Copper decreases for V and  $L_1$  fluid inclusions with  $T_h > 360^\circ\text{C}$  from 2700  $\mu\text{g/g}$  to less than 50  $\mu\text{g/g}$  for  $L_2$  fluid inclusions with  $T_h < 260^\circ\text{C}$ , and Fe decreases from 3000  $\mu\text{g/g}$  to 180  $\mu\text{g/g}$ . Lead concentrations between 150 – 60  $\mu\text{g/g}$  for  $L_1$  fluids decrease to less than 10  $\mu\text{g/g}$  for  $L_2$  FIAs; Zn concentrations decrease from 320 - 150  $\mu\text{g/g}$  in  $L_1$  FIAs to  $\sim 44$   $\mu\text{g/g}$  in  $L_2$  FIAs. Zinc and Fe are mostly below detection limit for  $L_2$  fluid inclusions ( $T_h < 270^\circ\text{C}$ ). Lead and zinc show large ranges of concentrations, but taking into account the large errors, these elements have no interpretable trend for the temperature range  $384^\circ - 340^\circ\text{C}$ . In the range  $340^\circ - 315^\circ\text{C}$ , values appear to be distinctly lower, but are hardly quantifiable due to uncertainties in the total salinity. Silver shows mostly low concentrations, between 10 and 1  $\mu\text{g/g}$ , in  $L_1$  FIAs and higher concentrations of up to 30  $\mu\text{g/g}$  in the lower temperature range  $L_2$  FIAs. Inverse trends to those of Cu, Fe, Zn and Pb can be recognised for As and Sb.  $L_1$  As values range from 180 to 30  $\mu\text{g/g}$ , slightly increasing from 50 to 200  $\mu\text{g/g}$  for  $L_2$  FIAs. Antimony shows no trend for  $L_1$  FIAs (mostly 50 - 25  $\mu\text{g/g}$ ) and a clear overall increase below for  $L_2$  FIAs (180 - 18  $\mu\text{g/g}$ ). Cs values are mostly constant in a range of 15 - 27  $\mu\text{g/g}$  for  $L_1$  FIAs. A clearly decreasing concentration trend is noted for  $L_2$  fluids at  $T_h 260^\circ\text{C}$  towards lower temperatures (45  $\mu\text{g/g}$  down to 4  $\mu\text{g/g}$ ), in concentrations as well as Cs/Na ratio. Recorded S values for high temperature assemblages of  $> T_h 360^\circ\text{C}$  are 1.1 - 0.38 wt%. For  $L_2$  inclusions S values strongly decrease and are mostly beyond detection limit. Sulphur concentrations for only a few single low temperature  $L_2$  fluid inclusions could be quantified (1200 and 2300  $\mu\text{g/g}$ ), indicating a sulphur concentration below 2300  $\mu\text{g/g}$ .

## 5. Discussion

### 5.1. P-T evolution of fluids and depth of vein formation

Microthermometry results record the history of vein formation in an open system with involvement of several fluid batches during the evolving hydrothermal system. A gradually cooler fluid of initially constant salinity of 4-5 wt% NaCl eq. but decreasing  $\text{CO}_2$  due to minor phase separation is recorded by  $L_1$  fluid inclusions attending initial base metal stage mineral precipitation. Increasing dilution/mixing with a similar but cooler fluid at  $T_h \sim 340^\circ\text{C}$  leads to a correlated drop in salinity and temperature down to about  $260^\circ\text{C}$  concluding base metal stage mineral precipitation. A boiling event at  $\sim 260^\circ\text{C}$  is registered by  $L_2$  boiling FIAs transiently raises the fluid salinity to 5.5 wt% NaCl eq. and initiates rhodochrosite precipitation of the carbonate stage. Mixing with another fluid causes salinity

to continue to drop, together with decreasing temperatures, to about 2 wt% NaCl eq. at 220° T<sub>h</sub>.

L<sub>1</sub> fluids contain CO<sub>2</sub> (3.1 - 5.2 mol%) which is gradually lost (T<sub>h</sub> <340°C) and below detection for L<sub>2</sub> FIAs post-dating the boiling event. CO<sub>2</sub> loss can be caused by small scale adiabatic boiling that would preferentially separate CO<sub>2</sub>, H<sub>2</sub>S and other volatiles from the fluid, which is supported by one registered boiling FIA at T<sub>h</sub> 327°C. Taken in account that minimum temperatures of vein formation are well above 300°C, this type of vein may be classified as a meso-epithermal ore.

High temperature L<sub>1</sub> CO<sub>2</sub>-bearing fluids have strongly varying minimum pressures (300 - 600 bar) theoretically suggesting a depth of about 4.5 km under purely hot hydrostatic pressure conditions, a conservative estimate, possibly over 6 km. More realistically, a partly lithostatic overload, as suggested by Roedder (1984), during the early stage of vein formation, would reduce the depth of formation, but it would still take place several (2-3) km below surface. A hydrostatic regime with intermittent sealing of the vein attaining lithostatic pressures could be proposed.

Absolute pressures calculated for the boiling event marked by precipitation of the rhodochrosite at about 260° are 39 - 47 bars, and correspond to 500 m depth under hot hydrostatic conditions. Considering that the sample was taken from a mine working 200 m below the surface, 300 m of overlying rock must have been eroded since this boiling event.

These results suggest that erosion of several km was necessary to telescope and expose the base metal veins to a near surface level, and that this exhumation took place during the lifetime of the base metal and carbonate stage of the vein.

## 5.2. *Evolution of base metal contents in the hydrothermal fluid*

The decrease of base metal concentrations in the fluid with temperature reflects the precipitation sequence of corresponding minerals within the vein paragenesis. Iron concentrations are the highest registered metal values and the rapid decrease in Fe concentrations corresponds to pyrite precipitation. A similarly clear trend is recognised for Cu and can be explained by tennantite-tetrahedrite precipitation. Although recognisable, a decrease in the Zn and Pb concentrations from L<sub>1</sub> to L<sub>2</sub> fluid inclusions is less clear. Zinc and lead mainly precipitate as sphalerite and galena at temperatures between 340° and 260°C.

Caesium and Cs/Na values are constant for the high temperature L<sub>1</sub> fluid inclusions within the T<sub>h</sub> range 260° - 380°C, indicating that the cooling fluid evolved from a similar fluid source in this temperature range, no dilution by a external fluid source occurred during cooling, and that decreasing metal concentration trends are likely to be precipitation trends. Caesium gives an indication of different fluids involved, because it is thought to be very incompatible and can therefore be used as an indicator of magmatic fluid origin (Audétat and Pettke, 2003; Audétat et al., 2008). At post-boiling temperatures of L<sub>2</sub> fluid inclusions (220° - 260°C) a declining trend of one order of magnitude is possibly caused by mixing with a Cs-poor fluid of non-magmatic origin (e.g. equilibrated meteoric water).

Similar decreasing metal values were found by Beuchat et al. (2004), applying microthermometry and LA-ICP-MS to single fluid inclusions in porphyry-related polymetallic vein ore in San Cristobal, Peru. He showed that element contents generally decrease with precipitation of the corresponding ore mineral. Kostova et al. (2004), show with the same techniques that Pb and Zn values in polymetallic veins in Madan, Bulgaria, decrease drastically in a restricted temperature range due to precipitation upon cooling. Decreasing metal contents of a metal-rich brine together with ongoing dilution by a low



salinity fluid, and precipitation of galena are documented from a metamorphic base metal deposit in Binn Valley, Switzerland (Klemm et al., 2004).

All metals are believed to be transported as chloride complex at epithermal temperatures, and their concentrations are expected to decrease with salinity (Hemley and Hunt, 1992; Seward and Barnes, 1997), or at higher temperatures, as a sulphur complex, especially for Cu (Seo et al., 2009).

Available base metal data from reserve calculations (personal comm. Pan American Silver Corp., 2006) allows a comparison of bulk ore data of the Jackeline vein and the metal values in the fluids from this vein. Pb/Zn ratios for bulk ore and fluid composition are very similar; both fall into the 1:1 to 1:12 range (Fig. 5a). The L<sub>1</sub> T<sub>h</sub> >340°C FIAs cluster together at higher concentrations, while the L<sub>2</sub> are mostly under LOD, except for one FIA showing lower values. An overall decreasing temperature trend is visible between the two groups. These Pb/Zn compositions are observed for a wide range of crustal fluids and might reflect the abundance of these metals in the crust (Yardley, 2005).

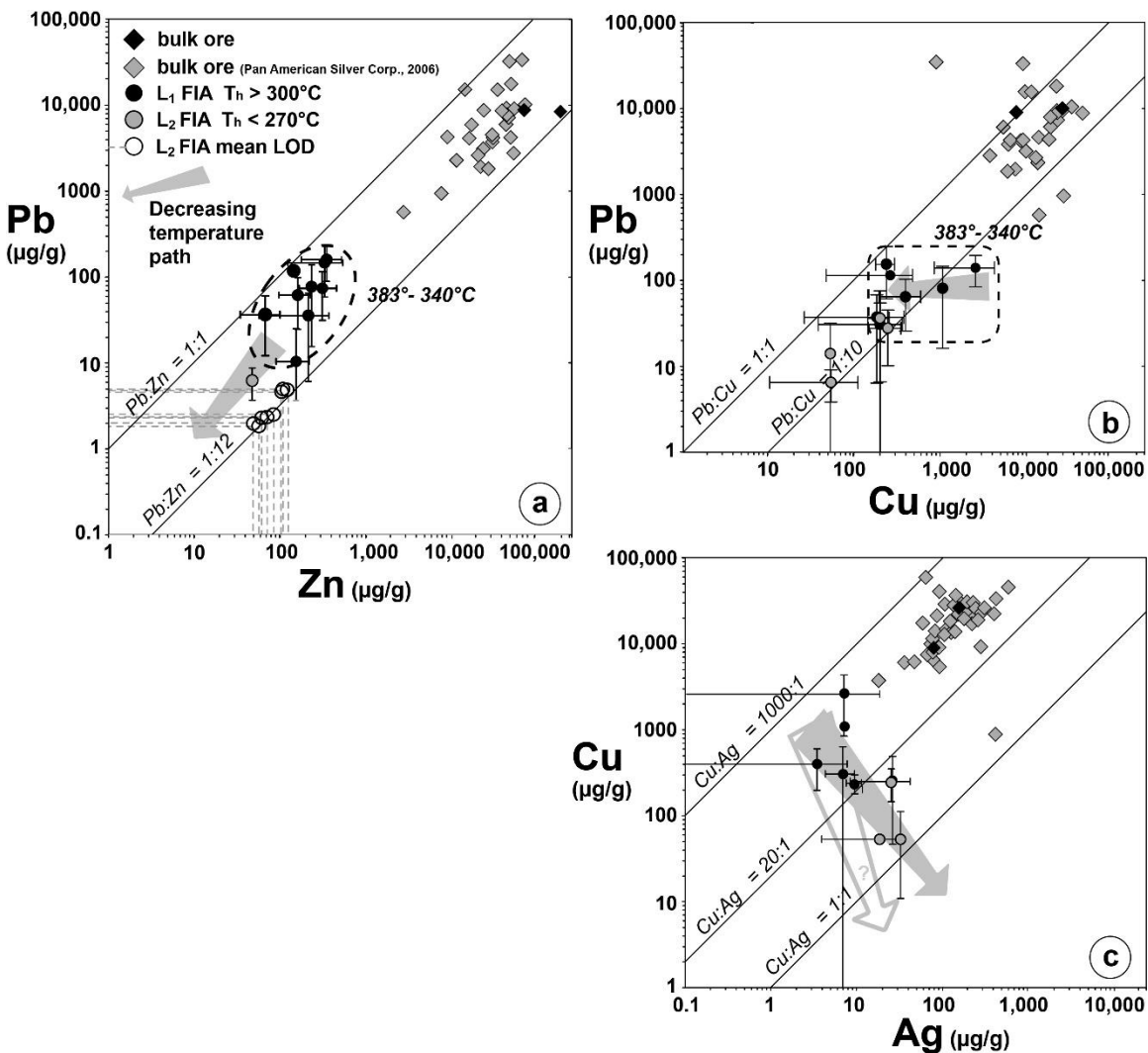


**Fig. 5.** Comparison of element concentrations in FIAs and bulk ore data from the Jackeline vein. Bulk ore as grey diamonds are calculated reserves from Pan American Silver Corp., black diamonds are bulk rock analyses of studied ore hand samples. Grey arrows indicate a general decrease in  $T_h$  for the FIA. Values for each FIA are plotted as mean with  $1\sigma$  error bars. Diagonal lines of equal element ratios are illustrated for reference.

A similar development can be observed for Pb/Cu values (Fig. 5b). Pb/Cu for fluids and bulk ore correspond well. Copper is relatively enriched in the early L<sub>1</sub> fluid inclusions compared to Pb, and later has constant Pb/Cu ratios (Fig. 8b). This is consistent with the observed continued precipitation of tennantite-tetrahedrite and galena in lesser quantities, after the bulk of galena and sphalerite precipitated. It is likely that most of the Cu precipitated from fluids with T<sub>h</sub> >340°C. Perhaps, hotter fluids were more influential in the formation of the Cu-rich ores in the core of the central part of the polymetallic Morococha district.

A positive Cu/Ag correlation trend of bulk ore can be readily explained by the presence of Ag in tennantite-tetrahedrite (0.3-1.4 wt%; unpublished electron microprobe data). Silver, in lesser amounts, is also found as Ag-telluride inclusions (hessite) in Ag-poor galena which affects the clearness of the correlation trend. Cu/Ag values show that fluid inclusions at high initial temperatures correspond to bulk ore data (Fig. 5c). During further cooling relative Ag enrichment becomes stronger. It appears that a part of the Ag remains in the fluid with decreasing homogenisation temperatures. It enriches relatively to Cu with decreasing T<sub>h</sub> (Fig. 5c), and does not precipitate abundantly during vein formation, but perhaps at a more distal position outwards and at lower temperatures (<220°C T<sub>h</sub>). Native Ag, Ag-sulphosalts and -sulphides can be found in more distal settings in the Morococha district, and fahlore and galena have higher Ag contents there, including small amounts of Au (Ageneau, 2008; Peréz, 2009).

### 5.3. Evolution of Sb and As in the fluid

The metalloids Sb and As show trends which are not comparable to the base metal trend. L<sub>2</sub> fluid inclusions have elevated concentrations for Sb and As, whereas the hotter, earlier L<sub>1</sub> fluids have slightly lower concentrations in average.

Experiments show that Sb and As in aqueous solution are not complexed with chlorine and sulphur ligands, but transported as the stable neutral hydroxyl complexes Sb(OH)<sub>3</sub> and As(OH)<sub>3</sub> in hydrothermal environments over a wide range of temperatures, and are very soluble even at low temperatures (Zotov et al., 1995; Pokrovski et al., 2002; Zotov et al., 2003). Therefore these elements do not correlate with fluid salinity.

Results from this study show that Sb and As remain in solution if not enriched in the post-boiling neutral pH L<sub>2</sub> fluids, at T<sub>h</sub> <260°C and are in equilibrium with carbonates. In contrast to Ag precipitating in distal settings of the district, Sb- and As-ores such as orpiment and stibnite have not been found suggesting that these elements precipitated in eroded parts of the hydrothermal system, or never precipitated, perhaps due to the lack of a sufficient amount of reducing sulphur (Williams-Jones and Normand, 1997), which is not available in the host rock or has been lost from the fluid. Stabilisation of Sb and As into the fluid can result from loss of H<sub>2</sub>S due to boiling or sulphide precipitation not involving Sb or As, shifting the equilibria of equation (1) and (2) towards the left side. The same effect could also be achieved by admixture of meteoric water.



Heinrich and Eadington (1986) report that Sb and As solubilities increase with higher oxidation state of the hydrothermal fluid, which could be the case for the low temperature, rock-reacted fluid with increasing amounts of more oxidised meteoric fluids.

#### 5.4. *Origin of the ore forming fluids*

Oxygen and hydrogen stable isotope studies on hydrous gangue minerals and fluid inclusions, considered to represent fluids forming porphyry-related Zn-Pb-Ag-Cu ore, have been studied in deposits such as Butte, USA (Zhang, 2000), and several deposits in Peru where porphyry intrusions are suspected, e.g.: Casapalca, (Rye and Sawkins, 1974), Cerro de Pasco (Baumgartner et al., 2008) and Colquijirca (Bendezú, 2007). The results indicate that the ore fluids could correspond to magmatic fluids with some degree of mixing with meteoric waters.

Magmatic fluids exsolve from solidifying magmatic bodies and can undergo phase separation into a coexisting dense brine and a low density vapour (Fournier, 1999; Ulrich et al., 1999). Pudack et al. (2009) and Kouzmanov et al. (2010) demonstrated on the basis of fluid inclusion microthermometry and LA-ICP-MS analyses that epithermal precious metal mineralisation can result from contracted vapour-type fluids of magmatic origin or mixing of vapour-type fluids with porphyry-type brines, respectively.

Several authors have proposed that the fluids in base metal veins similar to those of Morococha may result from strong dilution of porphyry brines with meteoric water, or from a single-phase magmatic fluid of intermediate density with variable degrees of mixing with meteoric water (Rusk et al., 2008a; Bendezú and Fontboté, 2009).

Sulphur content in the hydrothermal fluids can give an important indication about the fluid provenance. As outlined by Heinrich (2006) and Seo et al., (2009), the total sulphur budget of a magmatic derived fluid will control the degree of sulphide precipitation during its cooling path. As mentioned above, nearly all sulphides precipitated in the studied vein are pyrite (Fe), tennantite-tetrahedrite (Cu), sphalerite (Zn), and galena (Harris et al., 2008). The molality of total sulphur ( $m_{S,totM}$ ) necessary to precipitate all of these metals from the early fluid can be expressed as  $2 \cdot m_{Fe} + m_{Cu} + m_{Zn} + m_{Pb}$  corresponding to the composition of the sulphides and sulphosalts involved: pyrite ( $FeS_2$ ), tennantite ( $Cu_{12}As_4S_{13}$ ), sphalerite ( $ZnS$ ), galena ( $PbS$ ). Comparing  $m_{S,totM}$  with the total measured sulphur  $m_S$  in the fluid inclusions most of the FIAs are either equal or enriched in sulphur (Fig. 6). This demonstrates firstly, that the  $L_1$  fluids have the capacity to precipitate polymetallic ores. The availability of sufficient sulphur is usually assumed, but was as yet not confirmed. Secondly, this demonstrates that the early fluids have sufficient, if not excess, sulphur to precipitate all of the available metals in the fluid, even if some sulphur may have been lost due to  $H_2S$  degassing (volatile loss documented by  $CO_2$  decrease of  $L_1$  fluid inclusions). Diluted magmatic brines as origin for the hydrothermal fluid would require an additional source of sulphur to precipitate base metal sulphides, and are not likely to contribute in important proportions to the base metals in the fluid (Heinrich, 2006). Additionally, no strong initial variability in salinity was observed and only one brinal FIA directly related to polymetallic veins in the Morococha district identified (Catchpole, submitted). Salinity, density,  $CO_2$ - and metal content of the earliest registered  $L_1$  FIAs ( $383^\circ - 340^\circ C T_h$ ) resemble early B60 magmatic fluids from the barren quartz-pyrite veins predating the polymetallic Main Stage in Butte, Montana (Rusk et al., 2008b). These fluids are suspected to have contributed to the rich ores of the Main Stage mineralisation at Butte (Rusk et al., 2008a), which is very similar to the ores in Morococha presented in this study.

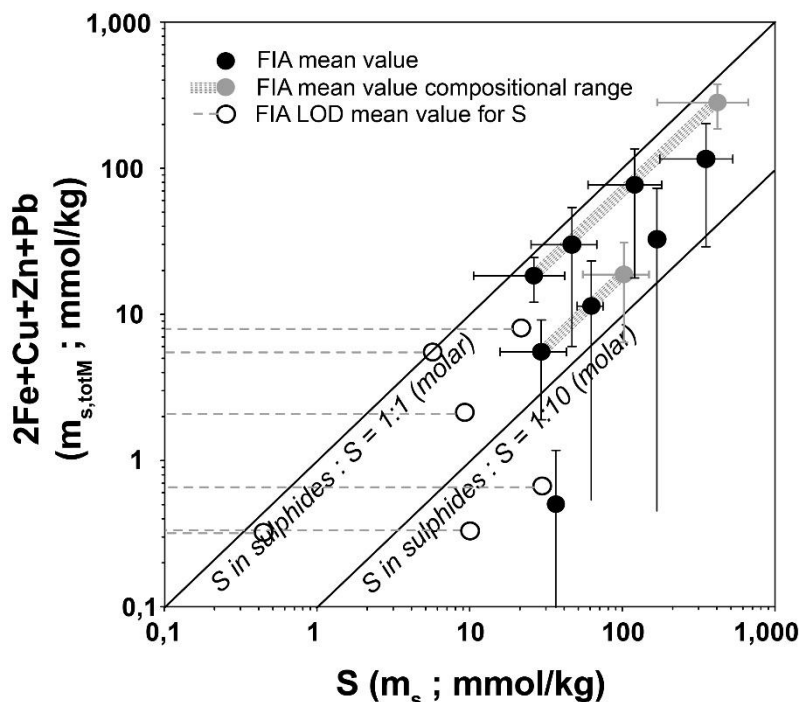


**Fig. 6.** Molalities of total measured sulphur ( $m_s$ ) in the fluid inclusions and sulphur in sulphides ( $m_{s,totM}$ ) necessary to hypothetically precipitate all Fe, Cu, Zn, and Pb in the fluid as pyrite ( $\text{FeS}_2$ ), tennantite ( $\text{Cu}_{12}\text{As}_4\text{S}_{13}$ ), sphalerite ( $\text{ZnS}$ ), and galena ( $\text{PbS}$ ), respectively. Mean values for all FIAs plotting on the  $m_s$  side of the 1:1 ( $m_{s,totM} : m_s$ ) line indicate relative enrichment of sulphur in the fluid. Dashed lines terminating in grey circles indicate LOD values for  $m_s$  for  $L_2$  FIAs post-dating rhodochrosite precipitation.

### 5.5. Comparison with other base metal deposits

Precipitation mechanisms of the evolving fluid and the effects of telescoping causing base metal zonation in the vein studied here are applicable to other porphyry-related base metal deposits which have very similar paragenetic patterns and important amounts of Cu, Zn, Pb, and Ag ores. Examples are the Main stage veins in Butte, USA (Meyer et al., 1968), the Victoria Cu-Zn-Au-Ag and Lepanto Cu-Au deposits, Philippines (Hedenquist et al., 1998; Hedenquist et al., 2001), and the base metal-rich deposits of Colquijirca (Bendezú and Fontboté, 2009), Cerro de Pasco (Baumgartner et al., 2008), and Casapalca in Peru (Wu and Petersen, 1977). Large mineralised Cu-Mo porphyry deposits with evidence for later meso-epithermal overprint of economically important Cu ores might also be included, such as Chuquicamata (Ossandón et al., 2001) and La Escondida (Ojeda, 1986; Padilla Garza et al., 2001), to name a few.

Volcanic-hosted massive sulphide deposits (VHMS) show base metal patterns corresponding to precipitation with decreasing temperature and mixing of upwelling base metal-loaded fluid with cool seawater (Franklin et al., 1981; Huston et al., 2010), which are processes (cooling and mixing) comparable to the ones observed for the porphyry-related base metal lode observed here.

One important characteristic of these porphyry-related fluids with magmatic signature is that they have sufficient reduced sulphur in solution to precipitate ores. Deposit types involving basinal brines, such as MVT and sediment-hosted Zn-Pb deposits, have precipitation mechanisms which are different from those studied here, because of the low sulphur content in the fluid or different speciation of the sulphur in solution, and depend on

mixing with a sulphur-rich fluid, pre-existing reduced sulphur in the host rock, or reduction of sulphate in solution for base metal precipitation (Stoffell et al., 2008; Wilkinson, 2010).

## 6. Conclusion

Fluid inclusions document the open system evolution of ore-forming fluids through the paragenesis of a single zoned base metal-rich vein in a retreating hydrothermal system with overprinting (telescoping) of mineral assemblages due to cooling and erosion.

Iron, Cu, Zn, Pb, and Ag precipitate from a fluid which shows decreasing salinity, temperature and CO<sub>2</sub> content, with initial values of 4-5 wt% NaCl eq., 340°- 380°C T<sub>h</sub>, and 3-5 mol% CO<sub>2</sub>, respectively. Precipitation is due to decreasing temperature and possibly boiling of the evolving fluid, while fluid mixing with an external source occurs at temperatures below ~260°C T<sub>h</sub>. Early base metal-rich fluids are probably magmatic, as suggested by Cs/Na values in the fluid, and have mixed with increasing amounts of equilibrated meteoric fluid below ~260°C T<sub>h</sub>, indicated by decreasing Cs/Na values and an ongoing stable isotope survey.

Evolution of the metal content in ore forming fluid V and L<sub>1</sub> to L<sub>2</sub> corresponds reasonably well to the observed depositional evolution of Fe, Cu, Zn, and Pb-bearing sulphides within the paragenesis of the polymetallic vein. Contrasting with decreasing metal values, concentrations of metalloids Sb and As are constant or slightly elevated in late fluids post-dating carbonate deposition, stabilised as neutral hydroxyl complexes in the fluid. Sulphur concentrations in the fluids are always sufficiently high to precipitate all metals in solution as sulphides. Metal zonation patterns and evolution of element abundances in the studied vein are also recognised on district scale showing a Cu-Fe-rich core area and Zn-Pb-Mn-Ag dominated ores in an intermediate to external position. Often documented As-Sb-Hg-Au ores in the outermost areas are absent in Morocochoa, but the high As and Sb values in the late fluids, even if never precipitated, support the district element zonation pattern.

Based on pressure calculations, the depth of emplacement is estimated to be at least several kilometres for the early base metal stage, whereas depth of the last mineral deposition is only several hundred meters below paleosurface. Erosional rates are therefore expected to be high, as several km of rock had to be eroded within the lifetime of the base metal and carbonate stage.

## Acknowledgments

This study was supported by the Swiss National Sciences Foundation (Grant 20020-108026) and the Pan American Silver Corp., providing field and logistical support, and access to the mine area. Pan American Silver Corp., Morocochoa staff is acknowledged for friendly support, Jung Hun Seo for support during the laser ablation work in Zurich and discussion, and Cindy Broderick for a detailed review and friendly comments. Thomas Driesner helped out with his crushing stage device. Discussions with John Dilles and Gleb Pokrovski contributed to ideas in the interpretation. We are grateful to Thomas Pettke for a detailed review which improved this paper.

## References

- Ageneau, M., 2008. Genesis of Ag-rich mineralisation in the Buenaventura and Galera veins, Yacumina zone, SW part of the Morococha district, central Peru, University of Geneva, 119 pp.
- Audétat, A., Günther, D. and Heinrich, C.A., 1998. Formation of a magmatic-hydrothermal ore deposit: Insights with LA-ICP-MS analysis of fluid inclusions. *Science*, 279: 2091-2094.
- Audétat, A. and Pettke, T., 2003. The magmatic-hydrothermal evolution of two barren granites: A melt and fluid inclusion study of the Rito del Medio and Cañada Pinabete plutons in northern New Mexico (USA). *Geochimica et Cosmochimica Acta*, 67(1): 97-121.
- Audétat, A., Pettke, T., Heinrich, C.A. and Bodnar, R.J., 2008. The composition of magmatic-hydrothermal fluids in barren and mineralized intrusions. *Economic Geology*, 103(5): 877-908.
- Bakker, R.J., 1997. Clathrates: Computer programs to calculate fluid inclusion V-X properties using clathrate melting temperatures. *Computers & Geosciences*, 23(1): 1-8.
- Bartos, P.J., 1989. Prograde and retrograde base metal lode deposits and their relationship to underlying porphyry copper deposits. *Economic Geology*, 84: 1671-1683.
- Baumgartner, R., Fontboté, L. and Vennemann, T., 2008. Mineral zoning and geochemistry of epithermal polymetallic Zn-Pb-Ag-Cu-Bi mineralization at Cerro de Pasco, Peru. *Economic Geology*, 103: 493-537.
- Bendezú, A., Catchpole, H., Kouzmanov, K., Fontboté, L. and Astorga, C., 2008. Miocene magmatism and related porphyry and polymetallic mineralization in the Morococha district, Central Peru, XIII Congreso Latinoamericano de Geología, Lima, Peru.
- Bendezú, R., 2007. Shallow polymetallic and precious metal mineralization associated with a Miocene diatreme-dome complex: the Colquijirca district in the Peruvian Andes. *Terre & Environnement*, 64: 221.
- Bendezú, R. and Fontboté, L., 2009. Cordilleran epithermal Cu-Zn-Pb-(Au-Ag) mineralization in the Colquijirca District, Central Peru: deposit-scale mineralogical patterns. *Economic Geology*, 104: 905-944.
- Beuchat, S., 2003. Geochronological, structural, isotopes and fluid inclusion constraints of the polymetallic Domo de Yauli District, Peru. *Terre & Environnement*, 41: 130.
- Beuchat, S., Moritz, R. and Pettke, T., 2004. Fluid evolution in the W-Cu-Zn-Pb San Cristobal vein, Peru: fluid inclusion and stable isotope evidence. *Chemical Geology*, 210(1-4): 201-224.
- Bodnar, R.J., Reynolds, T.J. and Kuehn, C.A., 1985. Fluid inclusion systematics in epithermal systems. In: B.R. Berger and P.M. Bethke (Editors), *Reviews in Economic Geology: Geology and geochemistry of epithermal systems*. Society of Economic Geologists, pp. 73-96.
- Bodnar, R.J. and Vityk, M.O., 1994. Interpretation of microthermometric data for H<sub>2</sub>O-NaCl fluid inclusions. In: B. de Vivo and M.L. Frezzotti (Editors), *Fluid inclusions in minerals, methods and applications*. Virginia Tech, Blacksburg, pp. 117-130.
- Brown, P.E., 1989. FLINCOR; a microcomputer program for the reduction and investigation of fluid-inclusion data. *American Mineralogist*, 74(11-12): 1390-1393.
- Catchpole, H., Bendezú, A., Kouzmanov, K., Fontboté, L. and Escalante, E., 2008. Multiple porphyry intrusion-centred base metal mineralisation styles in the Morococha district, central Peru, SEG-GSSA 2008 Conference, Johannesburg, South Africa.

- Cerro de Pasco Copper Corporation, 1948. Lead and zinc deposits of the Cerro de Pasco Corporation in central Peru, 18th International Geological Congress, Great Britain 1948, pp. 154-186.
- Diamond, L.W., 2001. Review of the systematics of CO<sub>2</sub> - H<sub>2</sub>O fluid inclusions. *Lithos*, 55: 69-99.
- Driesner, T., 2007. The system H<sub>2</sub>O-NaCl. Part II: Correlations for molar volume, enthalpy, and isobaric heat capacity from 0 to 1000 °C, 1 to 5000 bar, and 0 to 1 X<sub>NaCl</sub>. *Geochimica et Cosmochimica Acta*, 71(20): 4902-4919.
- Duan, Z., Møller, N. and Weare, J.H., 1992. An equation of state for the CH<sub>4</sub>-CO<sub>2</sub>-H<sub>2</sub>O system: II. Mixtures from 50 to 1000°C and 0 to 1000 bar. *Geochimica et Cosmochimica Acta*, 56(7): 2619-2631.
- Einaudi, M.T., Hedenquist, J.W. and Inan, E.E., 2003. Sulfidation state of fluids in active and extinct hydrothermal systems: Transition from porphyry to epithermal environments. *Society of Economic Geologists Special Publication*, 10: 285-313.
- Fournier, R.O., 1999. Hydrothermal processes related to movement of fluid from plastic into brittle rock in the magmatic-epithermal environment. *Economic Geology*, 94(8): 1193-1211.
- Franklin, J.M., Lydon, J.W. and Sangster, D.M., 1981. Volcanic-associated massive sulfide deposits. *Economic Geology 75th Anniversary Volume*: 485-627.
- Goldstein, R.H. and Reynolds, T.J., 1994. Systematics of fluid inclusions in diagenetic minerals. *Society for Sedimentary Geology Short Course 31*, Tulsa.
- Guilbert, J.M. and Park, C.F.J., 1986. Deposits related to intermediate to felsic intrusions - Cordilleran vein type deposits. In: J.M. Guilbert (Editor), *The geology of ore deposits*. W.H.Freemann and Company, New York, pp. 465-487.
- Guillong, M., Latkoczy, C., Seo, J.H., Günther, D. and Heinrich, C.A., 2008a. Determination of sulfur in fluid inclusions by laser ablation ICP-MS. *Journal of Analytical Atomic Spectrometry*, 23: 1581-1589.
- Guillong, M., Meier, D.L., Allan, M.M., Heinrich, C.A. and Yardley, B.W.D., 2008b. SILLS: a Matlab-based program for the reduction of Laser Ablation ICP-MS data of homogeneous materials and inclusions. In: P. Sylvester (Editor), *Laser-ablation-ICPMS in the earth sciences : current practices and outstanding issues*. Mineralogical Association of Canada, Vancouver, B.C., pp. 328-333.
- Günther, D., Audétat, A., Frischknecht, R. and Heinrich, C.A., 1998. Quantitative analysis of major, minor and trace elements in fluid inclusions using Laser Ablation-Inductively Coupled Plasma-Mass Spectrometry (LA-ICP-MS). *Journal of Analytical Atomic Spectrometry*, 13: 263-270.
- Harris, A.C. et al., 2008. Multimillion year thermal history of a porphyry copper deposit: application of U-Pb, <sup>40</sup>Ar/<sup>39</sup>Ar and (U-Th)/He. *Mineralium Deposita*, 43: 295-314.
- Hedenquist, J.W., Arribas, A.J. and Reynolds, T.J., 1998. Evolution of an intrusion-centered hydrothermal system: Far Southeast-Lepanto porphyry and epithermal Cu-Au deposits, Philippines. *Economic Geology*, 93(4): 373-404.
- Hedenquist, J.W., Claveria, R.J.R. and Villafuerte, G.P., 2001. Types of sulfide-rich epithermal deposits, and their affiliation to porphyry systems: Lepanto-Victoria-Far Southeast deposits, Philippines, as examples, Pro-Explo 2001, Congreso Internacional de Prospectores y Exploradores. Instituto de Ingenieros de Minas del Perú, Lima, pp. 29.
- Hedenquist, J.W. and Henley, R.W., 1985. The importance of CO<sub>2</sub> on freezing point measurements of fluid inclusions: evidence from active geothermal systems and implications for epithermal ore deposition. *Economic Geology*, 80: 1379-1406.



- Heinrich, C.A., 2006. From fluid inclusion microanalysis to large-scale hydrothermal mass transfer in the Earth's interior. *Journal of Mineralogical and Petrological Sciences*, 101: 110-117.
- Heinrich, C.A., Driesner, T., Stefánsson, A. and Seward, T.M., 2004. Magmatic vapor contraction and the transport of gold from the porphyry environment to epithermal ore deposits. *Geology*, 32(9): 761-764.
- Heinrich, C.A. and Eadington, P.J., 1986. Thermodynamic predictions of the hydrothermal chemistry of arsenic, and their significance for the paragenetic sequence of some cassiterite-arsenopyrite-base metal sulfide deposits. *Economic Geology*, 81(3): 511-529.
- Heinrich, C.A. et al., 2003. Quantitative multi-element analysis of minerals, fluid and melt inclusions by laser-ablation inductively-coupled-plasma mass-spectrometry. *Geochimica et Cosmochimica Acta*, 67(18): 3473-3496.
- Hemley, J.J., Cygan, G.L., Fein, J.B., Robinson, G.R. and D'Angelo, W.M., 1992. Hydrothermal ore-forming processes in the light of studies in rock-buffered systems: I. Iron-copper-zinc-lead solubility relations. *Economic Geology*, 87: 1-22.
- Hemley, J.J. and Hunt, J.P., 1992. Hydrothermal ore-forming processes in the light of studies in rock-buffered systems: II. Some general geologic applications. *Economic Geology*, 87: 23-43.
- Huston, D.L., Pehrsson, S., Eglington, B.M. and Zaw, K., 2010. The geology and metallogeny of volcanic-hosted massive sulfide deposits: variations through geologic time and with tectonic setting. *Economic Geology*, 105: 571-591.
- Klemm, L., Pettke, T., Graeser, S., Mullis, J. and Kouzmanov, K., 2004. Fluid mixing as the cause of sulphide precipitation at Albrunpass, Binn Valley, Central Alps. *Schweizerische Mineralogische und Petrographische Mitteilungen*, 84: 189-212.
- Klemm, L.M., Pettke, T., Heinrich, C.A. and Campos, E., 2007. Hydrothermal evolution of the El Teniente deposit, Chile: Porphyry Cu-Mo ore deposition from low-salinity magmatic fluids. *Economic Geology*, 102: 1021-1045.
- Kostova, B., Pettke, T., Driesner, T., Petrov, P. and Heinrich, C.A., 2004. LA ICP-MS study of fluid inclusions in quartz from the Yuzhna Petrovitsa deposit, Madan ore field, Bulgaria. *Schweizer Mineralogische und Petrographische Mitteilungen*, 84: 25-26.
- Kouzmanov, K. et al., 2008. The Miocene Morococha district, central Peru: large-scale epithermal polymetallic overprint on multiple intrusion-centered porphyry systems, PACRIM Congress 2008, Gold Coast, Queensland, Australia.
- Kouzmanov, K., Pettke, T. and Heinrich, C.A., 2010. Direct analysis of ore-precipitating fluids: Combined IR microscopy and LA-ICP-MS study of fluid inclusions in opaque ore minerals. *Economic Geology*, 105: 351-373.
- Landtwin, M.R. et al., 2010. The Bingham Canyon porphyry Cu-Mo-Au deposit. III. Zoned Copper-Gold ore deposition by magmatic vapor expansion. *Economic Geology*, 105: 91-118.
- McLaughlin, D.H. and Graton, L.C., 1935. Copper in the Cerro de Pasco and Morococha districts, Department of Junin, Peru., *Copper resources of the world (XVI International Geological Congress)*, pp. 513-544.
- Meyer, C., Shea, E., Goddard, C. and Staff, 1968. Ore deposits at Butte, Montana. In: J.D. Ridge (Editor), *Ore deposits of the United States 1933-1967*. American Institute of Minerals, Metals, and Petroleum Engineers, New York, pp. 1363-1416.
- Ojeda, J.M., 1986. The Escondida porphyry copper deposit, II Region, Chile: Exploration drilling and current geological interpretation *Mining Latin America*. Institution of Mining and Metallurgy, London, pp. 299-318.

- Ossandón, G., Fréaut, R., Gustafson, L.B., Lindsay, D.D. and Zentilli, M., 2001. Geology of the Chuquicamata mine: A progress report. *Economic Geology*, 96(2): 242-270.
- Padilla Garza, R.A., Tittley, S.R. and Pimentel, F., 2001. Geology of the Escondida porphyry copper deposit, Antofagasta region, Chile. *Economic Geology*, 96: 307-324.
- Peréz, J.A., 2009. Mineralization, structure and geochemical characteristics of the Toldojirca prospect and the San Andrés vein, Morococha district, Miocene polymetallic belt, Peru, University of Geneva, Geneva, 89 pp.
- Petersen, U., 1965. Regional geology and major ore deposits of central Peru. *Economic Geology*, 60(3): 407-476.
- Pokrovski, G.S. et al., 2002. Experimental study of arsenic speciation in vapor phase to 500°C: Implications for As transport and fractionation in low-density crustal fluids and volcanic gases. *Geochimica et Cosmochimica Acta*, 66(19): 3453-3480.
- Pudack, C., Halter, W.E., Heinrich, C.A. and Pettke, T., 2009. Evolution of magmatic vapor to gold-rich epithermal liquid: The porphyry to epithermal transition at Nevados de Famatina, Northwestern Argentina. *Economic Geology*, 104(4): 449-477.
- Roedder, E., 1984. Fluid inclusions. *Reviews in mineralogy*, 12. Mineralogical Society of America, 644 pp.
- Rosso, K.M. and Bodnar, R.J., 1995. Microthermometric and Raman spectroscopic detection limits of CO<sub>2</sub> in fluid inclusions and the Raman spectroscopic characterization of CO<sub>2</sub>. *Geochimica et Cosmochimica Acta*, 59(19): 3961-3975.
- Rusk, B.G., Miller, B.J. and Reed, M.H., 2008a. Fluid-inclusion evidence for the formation of Main Stage polymetallic base-metal veins, Butte, Montana, USA. In: J.E. Spencer and S.R. Tittley (Editors), *Arizona Geological Society Digest 22*. Arizona Geological Survey, Tucson, pp. 573-581.
- Rusk, B.G., Reed, M.H. and Dilles, J.H., 2008b. Fluid inclusion evidence for magmatic-hydrothermal fluid evolution in the porphyry copper-molybdenum deposit at Butte, Montana. *Economic Geology*, 103(2): 307-334.
- Rusk, B.G., Reed, M.H., Dilles, J.H., Klemm, L.M. and Heinrich, C.A., 2004. Compositions of magmatic hydrothermal fluids determined by LA-ICP-MS of fluid inclusions from the porphyry copper-molybdenum deposit at Butte, MT. *Chemical Geology*, 210: 173-199.
- Rye, R.O. and Sawkins, F.J., 1974. Fluid inclusion and stable isotope studies on the Casapalca Ag-Pb-Zn-Cu deposit, Central Andes, Peru. *Economic Geology*, 69: 181-205.
- Seo, J.H., Guillong, M. and Heinrich, C.A., 2009. The role of sulfur in the formation of magmatic-hydrothermal copper-gold deposits *Earth and Planetary Science Letters*, 282: 323-328.
- Seward, T.M. and Barnes, H.L., 1997. Metal transport by hydrothermal ore fluids. In: H.L. Barnes (Editor), *Geochemistry of hydrothermal ore deposits*. Wiley, pp. 435-486.
- Sillitoe, R.H., 2010. Porphyry Copper Systems. *Economic Geology*, 105: 3-41.
- Sterner, S.M. and Bodnar, R.J., 1984. Synthetic fluid inclusions in natural quartz I. Compositional types synthesized and applications to experimental geochemistry. *Geochimica et Cosmochimica Acta*, 48(12): 2659-2668.
- Stoffell, B., Appold, M.S., Wilkinson, J.J., McClean, N.A. and Jeffries, T.E., 2008. Geochemistry and evolution of Mississippi Valley-type mineralizing brines from the Tri-State and Northern Arkansas Districts determined by LA-ICP-MS microanalysis of fluid inclusions. *Economic Geology*, 103: 1411-1435.
- Ulrich, T., Günther, D. and Heinrich, C.A., 1999. Gold concentrations of magmatic brines and the metal budget of porphyry copper deposits. *Nature*, 399: 676-679.
- Wallier, S. et al., 2006. Magmatic fluids in the breccia-hosted epithermal Au-Ag deposit of Roşia Montană, Romania. *Economic Geology*, 101: 923-954.

- Wilkinson, J.J., 2010. A review of fluid inclusion constraints on mineralization in the Irish ore field and implications for the genesis of sediment-hosted Zn-Pb deposits. *Economic Geology*, 105: 417-442.
- Williams-Jones, A.E. and Normand, C., 1997. Controls of mineral paragenesis in the system Fe-Sb-S-O. *Economic Geology*, 92: 308-324.
- Wu, I. and Petersen, U., 1977. Geochemistry of tetrahedrite and mineral zoning at Casapalca, Peru. *Economic Geology*, 72: 993-1016.
- Yardley, B.W.D., 2005. Metal concentrations in crustal fluids and their relationship to ore formation. *Society of Economic Geologists 100th Anniversary Special Paper*, 100(4): 613-632.
- Zhang, L., 2000. Stable isotope investigation of a hydrothermal alteration system; Butte porphyry copper deposit, Oregon State University, 182 pp.
- Zhang, Y. and Frantz, J.D., 1987. Determination of the homogenization temperatures and densities of supercritical fluids in the system NaCl-KCl-CaCl<sub>2</sub>-H<sub>2</sub>O using synthetic fluid inclusions. *Chemical Geology*, 64: 335-350.
- Zotov, A.V., Kudrin, A.V., Levin, K.A., Shikina, N.D. and Var'yash, L.N., 1995. Experimental studies of the solubility and complexing of selected ore elements (Au, Ag, Cu, Mo, As, Sb, Hg) in aqueous solutions In: K.I. Shmulovich, B.W.D. Yardley and G.G. Gonchar (Editors), *Fluids in the crust - Equilibrium and transport properties*. Chapman & Hall, London, pp. 95-137.
- Zotov, A.V., Shikina, N.D. and Akinfiyev, N.N., 2003. Thermodynamic properties of the Sb(III) hydroxide complex Sb(OH)<sub>3(aq)</sub> at hydrothermal conditions. *Geochimica et Cosmochimica Acta*, 67(10): 1821-1836.